International Journal for Housing Science and Its Applications
Publish August 4, 2025. Volume 46, Issue 3 Pages 1576-1586

https://doi.org/10.70517/ijhsa463121

Flexible interconnection topology of low-voltage distribution network based on intelligent algorithm design and study of its strategy to adapt to new energy access

Linbo Wang[1,*], Yuanfeng Wang[1], Xi Zeng[1], Enwei Wang[1], Lei Lv[1], Fan Zhang[2] and Shuai Zhao[2]
[1] Guizhou Grid Co., Ltd. Guiyang Power Supply Bureau, Guiyang, Guizhou, 55000, China
[2] China Southern Power Grid Artificial Intelligence Technology Co., Ltd., Guangzhou, Guangdong, 510555, China
Corresponding authors: (e-mail: 17728117081@163.com).

Abstract In this study, a flexible interconnection topology design method based on intelligent algorithm-driven design is proposed for the flexibility and stability needs of low-voltage distribution networks in new energy high-penetration scenarios, and new energy access strategies are optimized by combining with the honeycomb active distribution network (HADN) structure. By improving the Davignan equivalent impedance voltage drop model and introducing the relative electrical distance matrix, the fast calculation of the static voltage stability index (SVSI) of the distribution network is realized, which reduces the computational complexity of topology optimization. The designed HADN topology supports active/reactive power optimization by realizing dynamic energy mutualization and cooperative protection among microgrid clusters through smart power exchange base stations (SPIES). Simulation experiments show that the proposed strategy has good adaptability under complex operating conditions, with PV power prediction accuracies of 93.14% day-ahead and 98.86% intraday, and unregulatable load prediction accuracies of 86.18% (day-ahead) and 96.34% (intraday), respectively. In the steady state operation, each distributed power source (DG) stabilizes rapidly, of which the combined photovoltaic battery system, photovoltaic power generation system, fuel cell and wind power generation system reach the steady state within 1s, 0.5s, 0.3s and 4s, respectively.

Index Terms low voltage distribution network, honeycomb active distribution network, flexible interconnection topology, static voltage stabilization, new energy access

I. Introduction

In recent years, due to the large consumption of fossil fuels and other traditional fuels, global warming, the greenhouse effect and other problems are becoming more and more serious, so China has made a commitment to “carbon peak, carbon neutral” in the United Nations General Assembly. As one of the important components of the energy system of the power system, to create a new power system mainly based on renewable energy is an important way to realize the “dual carbon” goal [1], [2]. For this reason, the source-load characteristics of the new power system have also been changed, and on the power and load sides, the distributed energy sources mainly based on photovoltaic power generation and the new loads mainly based on fast charging stations for electric vehicles are gradually connected to the power system on a large scale [3], [4]. Given that the above new source loads are characterized by high stochasticity and volatility, distribution grids with inherent single-radial topology will face a variety of power quality problems such as high harmonic current content, three-phase current asymmetry, and node voltage overruns [5]-[7].

In order to improve the power quality of low-voltage distribution networks and solve the voltage overrun problem, the traditional regulation means are mainly adding passive filters, adjusting on-load voltage regulators, and installing contact switches [8]. However, these programs have poor flexibility, insufficient regulation range and response speed, and are difficult to cope with the demand for distribution network operation and regulation under the extensive access of new source loads [9], [10]. On the other hand, flexible distribution network is based on the traditional distribution network, through the flexible modification of some key nodes or branch circuits, so as to make it have flexible closed-loop capability [11]. Flexible distribution network can significantly improve the quality and reliability of power supply and effectively cope with the volatility problems arising from the access of distributed power sources and DC loads, so the flexible development of low-voltage distribution network is an inevitable trend [12], [13].

In order to solve the problems of insufficient local power capacity and source charge mismatch in low-voltage distribution networks when large-scale distributed energy sources are connected, a large number of scholars have analyzed the flexible interconnection structure of AC and DC distribution networks. Wu, T. et al. established a two-

terminal power supply type topology suitable for tidal current complementation using a back-to-back flexible interconnection device, utilizing which smooth switching between the two operating methods is possible during normal operation and during a single-side fault [14]. Yuan, M. et al. proposed the use of a series flexible interconnection structure for the transformation of a power system with large-scale distributed energy access, and further proposed an effective valve control system and drive module by analyzing the topology and control principle of this system [15]. At the same time, some scholars have also accurately assessed the overall performance of distribution grids under different flexible interconnection topologies with the help of intelligent optimization models, which provides a solid data base for reliable operation and future planning of the grid. Li, J. et al. investigated a coordinated planning method for flexible interconnection devices and distributed energy storage systems in low-voltage distribution networks, and effectively improved the storage capacity and transmission power of distributed energy sources when accessing them by establishing a two-layer planning model with the objective of minimizing the integrated cost and energy abandonment [16]. Zu, G. et al. proposed to construct a model of the relationship between the total supply capacity of the distribution network and the capacity of the low-voltage flexible interconnection device for the flexible trend control and multilevel load transfer phenomena existing in the low-voltage flexible distribution network, and to provide guidance for the planning and operation of the distribution network under the distributed energy access with the help of the branch demarcation algorithm [17]. Yang, Y. et al. developed an interconnection planning model for distribution grids with multiple microgrids based on connection type, investment cost, and operation scheduling, and used a two-layer optimization algorithm to solve for the optimal interconnection structure to achieve the maximum economic benefits [18].

Taking the low-voltage distribution network as the research object, this study combines intelligent algorithms and power electronics technology to propose a topology design method for flexible interconnected smart distribution networks, and focuses on solving the core problems of its static voltage stability analysis, topology optimization, and cooperative control of interconnected microgrids. Based on the fast calculation of static voltage stability index (SVSI) of distribution networks, an improved Davignan equivalent impedance voltage drop model is proposed, which reduces the computational complexity through the relative electrical distance matrix and provides a real-time stability assessment basis for topology design. Aiming at the flexibility and reliability requirements of new energy access, a honeycomb active distribution network (HADN) topology is designed to realize energy mutualization and cooperative protection among microgrid clusters by means of smart power exchange base stations (SPIES). The honeycomb active distribution network is composed of distributed microgrids with standardized configurations, each of which realizes regional autonomy in the integrated mode of “source-network-load-storage”, and adjacent microgrids are interconnected to form a honeycomb structure through SPIES. SPIES implements power bidirectional flow control based on power electronic devices (e.g., bidirectional DC/AC converters) to support active/reactive power optimization and energy mutualization among microgrids. It also constructs a layered control system for interconnected microgrids and proposes a power interaction controller model based on voltage source converter (VSC) to ensure the stable operation of multi-microgrid systems under dynamic operating conditions.

II. Intelligent algorithm-driven flexible interconnection topology design and stability study of low-voltage distribution networks

II. A.Indicators of static voltage stability in distribution networks

There is a complex coupling between static voltage stability and active and reactive power in the distribution network.The PV curve reflects the relationship between node active power changes and voltage.Although there is no explicit expression of the relationship between voltage and reactive power, the PV curve is generally obtained by the continuous tidal current method, which has already taken into account the influence of reactive power on voltage in the distribution network.The state of saddle-node bifurcation point of the PV curve corresponds to the tidal current equation The Jacobi matrix appears to have zero eigenvalue, so the saddle-node bifurcation point of the PV curve is the critical stabilization point of the system static voltage.

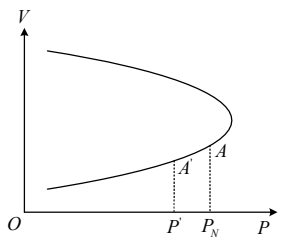

Figure 1: Power system PV curve

Figure 1 shows a schematic diagram of the PV curve of a power system, reflecting the relationship between the power consumed by a load in the power system, P, and the variation of the voltage, V, at that load.

For constant power loads, the system should supply rated power P_N to the load when the system is operating normally at point A in the lower half of the PV curve. If the load-side voltage is reduced by perturbation, the system provides power to the load with too low a value of P, and insufficient active power supplied by the system leads to a further reduction of the load-side voltage to reach the position of A', which creates a vicious circle and exacerbates the power imbalance.

According to the Davignan equivalent circuit, when the line is at the maximum load, i.e., the saddle-knot bifurcation point of the PV curve, the load-side voltage is equal to the voltage on the Davignan equivalent impedance, so that the saddle-knot bifurcation point can be solved quickly, avoiding the drawbacks of non-convergence of the trend equation, complicated calculation and slow speed in the continuous tidal current method. In this paper, we propose to use an iterative algorithm to determine the distance matrix, where the m th column in the matrix denotes all paths between bus m and the generator controlling the voltage of that bus. The voltage ΔV_n on the Davignan equivalent impedance is computed from the port voltage of the PV-type generator closest to the bus m and the load side voltage.

The operating condition of the power system changes all the time, and when the topology of the distribution network changes it is necessary to re-calculate the iteration matrix for each bus, which is more expensive to calculate. Therefore, relative electrical distance is introduced to list the voltage-current relationship between generator buses and load buses, as shown in Equation (1).

$$\begin{bmatrix} V_L \\ I_G \end{bmatrix} = \begin{bmatrix} Z_{LL} & F_{LG} \\ K_{GL} & Y_{GG} \end{bmatrix} \begin{bmatrix} I_L \\ V_G \end{bmatrix} \tag{1}$$

where: V_L is the load bus voltage matrix; I_G is the generator grid-connected bus current matrix; I_L is the load bus current matrix; V_G is the generator grid-connected bus voltage matrix; F_{LG} and K_{GL} denote the electrical relationship between the generator and load bus. The electrical relationship between the generator and the load bus can be derived from the nodal admittance matrix; Z_{LL} and Y_{GG} are the submatrices of the impedance and admittance matrices at the corresponding positions in the impedance and admittance matrices. The relative electrical distance matrix R_{LG} can be calculated using the matrix F_{LG} as shown in Equation (2).

$$R_{LG} = A - abs[F_{LG}] = A - abs[|Y_{LL}|^{-1}|Y_{LG}|] \tag{2}$$

where: A is an all-1 matrix of the same dimension as R_{LG}; abs denotes the absolute value taken for the elements within the matrix; Y_{LL} and Y_{LG} are submatrices of the corresponding positions in the conductivity matrix.

The elements in R_{LG} denote the relative electrical distances of the load from all generators in the system, which is computationally significantly less intensive compared to the shortest path determination method via iterative matrices.

Comparing the size of the elements in each column of the matrix R_{LG}, the generator closest to the specified bus can be determined to calculate the Davignan equivalent impedance voltage drop ΔV_∞ as shown in Equation (3).

$$\Delta V_\infty = \sum_{q=M} |\vec{V}_q - \overrightarrow{V_{q+1}}| \cong |\vec{V}_g - \vec{V}_l| \tag{3}$$

where: m is the bus serial number; M is the set of all buses in the shortest path from generator g to load bus l determined by the iterative method; $\vec{V}_q$ is the voltage on bus q; $\vec{V}_g$ is the voltage at the end of the generator g which has the shortest relative electrical distance; $\vec{V}_l$ is the load bus l voltage.

Different voltage stabilization indexes are subject to some degree of error due to different approximations taken. When a bus in the power system is in the critical stable state of voltage, the adjacent bus voltage will also produce a large voltage fluctuation phenomenon, so the correction factor β is added, as shown in Equation (4).

$$\beta = 1 - (\max |V_{\max} - V_{\min}|)^2 \tag{4}$$

where: $V_{\max}$ is the highest bus voltage standard value in the system; $V_{\min}$ is the lowest bus voltage standard value in the system. The simplified voltage stability index (SVSI) calculation formula is shown in equation (5).

$$S_{VSI}^{\infty} = \frac{\Delta V_{\infty}}{\beta V_{\infty}} \tag{5}$$

where: S_{VSI}^{∞} is the simplified voltage stability index of bus m; V_{∞} is the voltage at bus m.

When $S_{VSI}^{\infty} = 1$, it means that bus m is in the critical stable state of voltage. After calculating all bus S_{VSI}^{∞} values, the maximum of them is selected to indicate the voltage stability of the distribution network.

When the overexcitation current limiter and stator current limiter work in the generator, the generator loses voltage control and enters into the PQ operation mode, emitting a fixed amount of active and reactive power. Therefore the calculation of SVSI index for each bus requires rewriting the node conductance matrix to reconfirm the PV type generator closest to that bus.

II. B. Topology design of flexible interconnected smart distribution grid

Fast calculation based on static voltage stability index provides real-time stability criterion for distribution network topology optimization. However, the traditional radial topology is difficult to meet the flexible demand in new energy high penetration scenarios. Therefore, this section further proposes a honeycomb active distribution network (HADN) topology, which realizes dynamic energy interactions among microgrid clusters through flexible interconnection devices.

II. B. 1) Concept and structural characteristics of flexible interconnected smart distribution grids

As the use of flexible interconnection of large-scale power electronic equipment expands, the distribution network structure is developing from a basic radial type to a multi-terminal interconnection type network, and the power distribution mode is gradually evolving from a basic AC system to a hybrid AC/DC form. Multi-terminal flexible AC/DC hybrid distribution network based on flexible DC technology is beneficial to the flexible access of various distributed power sources and electric vehicles, and also provides the basic conditions and core equipment for the construction of flexible smart distribution network. The large number of microgrid technology has become the development direction of intelligent distribution grid for distributed system in the future. Flexible interconnection intelligent distribution grid is to connect each feeder, each AC/DC distribution electronic network or microgrid (group) in the distribution grid through flexible interconnection device (FID), so that each distribution electronic network or microgrid (group) gives full play to its own characteristics, realizes the distributed new energy, energy storage equipment, electric vehicles, etc., and realize intelligent scheduling among the distribution networks or microgrids (groups) to achieve the functions of trend control, energy mutual aid, active and reactive power optimization, and cooperative protection. The currently proposed honeycomb active distribution network is a flexible interconnected smart distribution network.

II. B. 2) Cellular active distribution network topology

The honeycomb active distribution network is a distributed microgrid cluster with standardized configuration of “source network and load”, which is combined into a network with a honeycomb structure through Smart Power/Information Exchange Base Stations (SPIES), hereinafter referred to as Base Stations, to realize regional autonomy of microgrids and wide urban interconnection among them. Neighboring microgrids utilize power electronic-based controllable devices to achieve power inter-supply, thus weakening the electrical connection to the main grid. Specifically, each microgrid constitutes an autonomous small/micro power supply and use system through the standardized configuration of “source grid, load and storage”, thus realizing the local consumption of new energy and the basic self-balancing of supply and demand within the region to the greatest extent possible, and the residual/shortage of power can be exchanged freely with the adjacent microgrids through the controllable equipments distributed in the district; the whole power distribution system will be composed of The whole distribution system will be formed by a cluster of relatively independent and interconnected distributed autonomous microgrids. This constitutes a honeycomb active distribution network (HADN) topology, with no electromagnetic loop between the microgrid clusters, which has the advantages of strong network architecture, strong ability to consume clean energy, flexible distribution methods and support for power market transactions.

The honeycomb active distribution network topology is composed of multiple microgrids, and neighboring microgrids are interconnected with power electronics-based base stations through their respective public connection points (PCCs), thus forming the whole honeycomb active distribution network as shown in Fig. 2. Under normal operation, the power supply and demand of the microgrids (including energy storage) are essentially balanced with the load of each microgrid; when power anomalies or faults occur in the microgrids, each relevant base station can

quickly scatter an accurate assessment based on the monitored situation, and according to the results of the assessment, apply power support in time to restore the balance or choose to disconnect from the faulty microgrid.

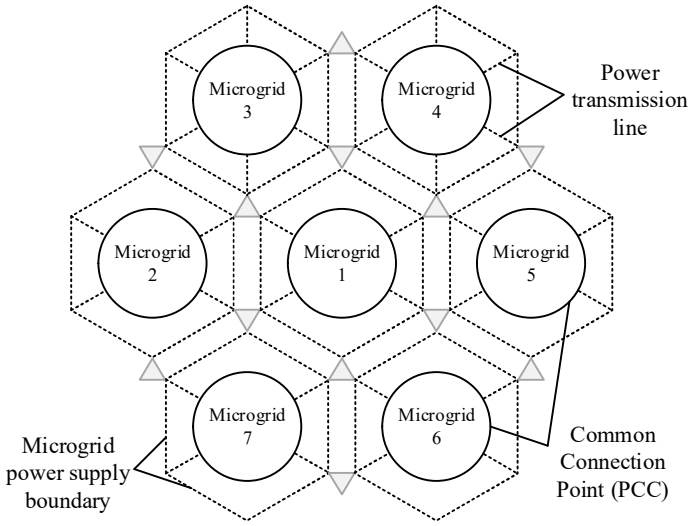

Figure 2: Topology of honeycomb active distribution network

Each microgrid in the honeycomb active distribution network topology requires six base stations to provide power support, and each base station liaises with three microgrids. The number of base stations required is high, the construction cost is relatively high, and the communication and decision-making mechanisms between multiple base stations and microgrids are complex. The relay protection configuration of the honeycomb active distribution network is also more complex than that of the traditional distribution network with open-loop operation, so the honeycomb active distribution network can be improved to construct a better topology.

II. C.Interconnected microgrid stability study

Although the honeycomb topology enhances the new energy consumption capacity, its multi-microgrid interconnection architecture needs to solve the stability problem under dynamic operating conditions. To this end, this section investigates the power interaction and cooperative control of interconnected microgrids, and proposes a hierarchical control strategy based on VSC to ensure the robust operation of the system under complex disturbances.

II. C. 1) Interconnected microgrid power interaction controllers

Electrical connectivity between microgrids and microgrids is established through interconnected power bidirectional converters to control the power dispatch between microgrids. In this paper, a power interaction controller between interconnected microgrids is proposed based on voltage source converter (VSC). The controller principle is introduced through the equivalent circuit of power interaction between the two buses, which is shown in Fig. 3.

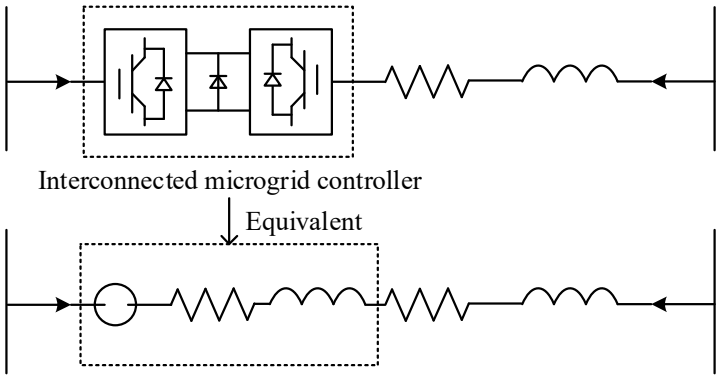

Figure 3: Equivalent circuit model of interconnected bus bars

According to Kirchhoff's law, the expression for the current flowing from bus i to bus j:

$$I_i = \frac{U_i - U_j - U_b}{(R + R_b) + j(X + X_b)} \tag{6}$$

Considering the ability of the interconnection controller to power interaction between buses, its current I_i is decomposed into I_i^1 and I_i^2, i.e., $I_i = I_i^1 + I_i^2$, where the current due to the difference in potential of the two buses without considering the interconnection controller is I_i^1 expression :

$$I_i^1 = \frac{U_i - U_j}{R + jX} \tag{7}$$

Therefore, the expression for the influence current I_i^2 of the interconnection controller:

$$I_i^2 = I_i - I_i^1 = \frac{U_i - U_j - U_b}{(R + R_b) + j(X + X_b)} - \frac{U_i - U_j}{R + jX} \tag{8}$$

where $I_j = -I_i$, and identically:

$$I_j^1 = \frac{U_j - U_i}{R + jX} \tag{9}$$

$$I_j^2 = I_j - I_j^1 = -\frac{U_i - U_j - U_b}{(R + R_b) + j(X + X_b)} - \frac{U_j - U_i}{R + jX} \tag{10}$$

Let $Z = R + jX$, which simplifies to:

$$\begin{bmatrix} I_i \\ I_j \end{bmatrix} = \begin{bmatrix} \frac{1}{Z} & -\frac{1}{Z} \\ -\frac{1}{Z} & \frac{1}{Z} \end{bmatrix} \begin{bmatrix} U_i \\ U_j \end{bmatrix} + \begin{bmatrix} I_i^2 \\ I_j^2 \end{bmatrix} \tag{11}$$

where U_i, U_j, U_b are the voltages at the i th and j th bus terminals and the interconnection controller, respectively; The I_i, I_j are the currents flowing from the bus i and j to the feeder, respectively; R, R_b are the resistances of the feeder and controller, respectively; X, X_b are the reactances of the feeder and controller, respectively. Where let $Z_T = (R + R_{bb}) + j(X + X_{bb})$, the power injection model can be expressed:

$$\begin{aligned} P_i &= \frac{1}{Z_T}\left\{\begin{matrix} \frac{Z_b}{Z}\left[U_i U_j \cos(\theta_{Z_b} + \delta_j - \delta_i - \theta - \theta_T)\right] - U_i^2 \cos(\theta_{Z_b} - \theta - \theta_T) \\ -U_b U_i \cos(\delta_b - \delta_i - \theta_T) \end{matrix}\right\} \\ &= \frac{U_i}{Z_T}\left\{\frac{Z_b}{Z}\left[\sum_{n \in i,j} U_n \cos(\theta_{Z_b} + \delta_n - \delta_i - \theta - \theta_T)\right] - U_b \cos(\delta_b - \delta_i - \theta_T)\right\} \end{aligned} \tag{12}$$

$$\begin{aligned} Q_i &= \mathrm{Im}(U_i (I_i^2)^*) \\ &= \frac{1}{Z_T}\left\{\begin{matrix} \frac{Z_b}{Z}\left[U_i U_j \sin(\theta_{Z_b} + \delta_j - \delta_i - \theta - \theta_T)\right] - U_i^2 \sin(\theta_{Z_b} - \theta - \theta_T) \\ -U_b U_i \sin(\delta_b - \delta_i - \theta_T) \end{matrix}\right\} \\ &= \frac{U_i}{Z_T}\left\{\frac{Z_b}{Z}\left[\sum_{n \in i,j} U_n \sin(\theta_{Z_b} + \delta_j - \delta_i - \theta - \theta_T)\right] - U_b \sin(\delta_b - \delta_i - \theta_T)\right\} \end{aligned} \tag{13}$$

Similarly, the bus j can be injected with active and reactive power:

$$P_j = \frac{U_j}{Z_T}\left\{\frac{Z_b}{Z}\left[\sum_{nei,j} U_n \cos(\theta_{Z_b} + \delta_n - \delta_j - \theta - \theta_T)\right] - U_b \cos(\delta_b - \delta_j - \theta_T)\right\} \quad (14)$$

$$Q_j = \frac{U_j}{Z_T}\left\{\frac{Z_b}{Z}\left[\sum_{nei,j} U_n \sin(\theta_{Z_0} + \delta_n - \delta_j - \theta - \theta_T)\right] - U_b \sin(\delta_b - \delta_j - \theta_T)\right\} \quad (15)$$

where P_i, Q_i, P_j, Q_i are the active and reactive power injected into bus i and bus j, respectively: $\theta, \theta_\tau, \theta_{Z_b}$ are the real-time phases, respectively, Davignan equivalent circuit phase, and interconnection controller phase; $\delta_i, \delta_j, \delta_b$ are the phase angles of bus i, bus j, and interconnection controller, respectively.

II. C. 2) Interconnected microgrid hierarchical control structure

The control strategy for the stable operation of the multi-microgrid distribution system is divided into two parts, mainly containing the micro-source control level and the microgrid control level. Micro-source control refers to maintaining the stable operation of the system through the output power control of distributed power sources to guarantee the stability of the system frequency and voltage. Microgrid control level refers to the power scheduling control strategy between interconnected microgrids and microgrids and power grids, which realizes the power exchange between microgrids through the central control center (MGCC), and the basic unit of control is the microgrid system, and the control methods can be divided into four control strategies: multi-agent control, peer-to-peer control on the microgrid level, master-slave control on the microgrid level, and hierarchical control on the microgrid level. The traditional multi-microgrid double-layer or three-layer control system is the normal operating state to the economy as the goal, reasonable scheduling of power flow between the microgrid and the main grid, to overcome the uncertainty of renewable energy generation fluctuations, improve the utilization rate of new energy power generation, and achieve the optimal scheduling of the power of the multi-microgrid system.

III. Dynamic modeling and simulation of flexible interconnected microgrids

Through the theoretical analysis of the intelligent algorithm-driven flexible interconnection topology design and stability strategy in Chapter 2, in order to verify its applicability under actual complex working conditions, this chapter further constructs a dynamic model of flexible interconnection microgrid and carries out a multi-scenario operation verification based on the simulation experimental platform, so as to comprehensively evaluate the dynamic response characteristics and steady state performance of the proposed topology and control strategy.

III. A. Microgrid modeling

The load parameters are shown in Table 1. The flexible interconnected microgrid system constructed in this paper, the voltage level of 380V, frequency of 50Hz microgrid through a step-up transformer connected to the 10kV medium voltage distribution network, in which the transformer wiring form of Dynll, capacity of 400kVA, the transformer secondary side winding neutral point by 30 resistance grounding. The wiring of the power lines are three-phase four-wire system, the type of line is divided into six categories: node 1 to node 9 of the line between the line for the line type, the distance between the two neighboring nodes for 35m; node 3 and node 12 of the line between the line for the line type two, the distance between the two neighboring nodes for 20m; node 3 to the load, node 12 to the load, node 5 to the load, as well as nodes 2 and 9 to the load of the lines are line three, line four, line five and line six types, respectively. The neutral line resistance value R_{neural}, which is not labeled in the line parameters, is the same as the phase impedance $R_{ph}+jX_{ph}$. There are six access loads in the microgrid, and the loads are set as three-phase balanced loads to simplify the system model.

Table 1: Micro network load parameters

	Access node	Active load (kW)	Reactive load (kvar)
Load 1	L1	100	50
Load 2	L2	150	100
Load 3	L3	150	100
Load 4	L4	100	50
Load 5	L5	150	100
Load 6	L6	200	120

III. B. Simulation experiment analysis

Based on the detailed model of the flexible interconnected microgrid established in Section 3.1, this section analyzes the dynamic behavior of the system under different scheduling strategies and operating states, including day-ahead/intra-day optimized scheduling and steady-state operation scenarios, through simulation experiments to quantitatively assess the flexibility and robustness of the designed topology.

III. B. 1) Analysis of day-ahead and intra-day scheduling

An energy management strategy analysis is conducted for the AC and DC multi-distribution feeder flexible interconnection system dispatch center. The system consists of three AC lines and one DC line, which are interconnected by three flexible interconnection devices (FIDs) with capacities of 150kW, 120kW, and 100kW; one photovoltaic power plant (PV) with a generating capacity of 80kW; and two battery energy storage (BES) with capacities of 50kW and 30kW, respectively; Includes a variety of loads such as non-adjustable loads (important loads), interruptible loads, and leveling loads.

The daily forecast, intraday forecast and actual measured values of light intensity are shown in Figure 4. The green segment dashed line is the day-ahead prediction, the purple dot-dashed line is the intraday prediction, and the orange solid line is the actual measurement.

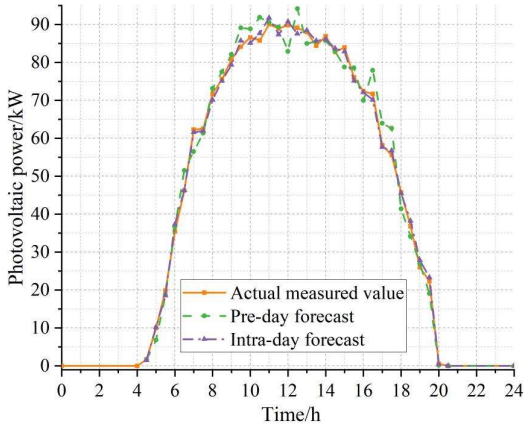

Figure 4: The pre-day, intra-day predicted value and actual value of light intensity

It can be seen that the error between the predicted value and the actual measured value is not high, and the accuracy of PV power prediction reaches more than 90%, in which the error of intraday prediction value is smaller than that of the prediction value before the day, with the accuracy of intraday prediction reaching 98.86%, and the accuracy of prediction before the day is 93.14%, and the PV prediction error is large for the noon time as well as the sunset time from 16:00 to 18:00.

In accordance with the energy management method, the dispatch of controllable loads such as interruptible loads and leveling loads is determined through the day-ahead optimal dispatch and passed to the intraday optimal dispatch succession, and the resulting day-ahead forecasts of only interruptible loads and leveling loads and other controllable loads are shown in Fig. 5.

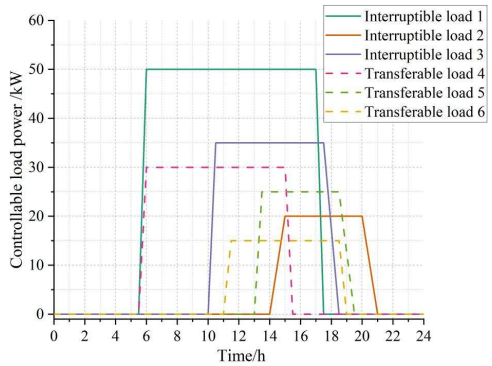

Figure 5: Day ahead forecast of controllable load

From the day-ahead forecasts of controllable loads, interruptible load 1 stays under 50kW of load power from 6:00-17:00, interruptible load 2 and interruptible load 3 stabilize under 20kW and 35kW from 15:00-20:00 and 10:30-17:30, respectively, and pannable load 4 stays under 30kWkW of load power from 6:00-15:00 under the load power, and panable loads 5 and 6 stabilized at 25kW and 15kW from 13:30-18:30 and 11:30-18:30, respectively.

In addition the day-ahead forecast, intraday forecast and actual measured values of the non-adjustable loads (significant loads) are shown in Fig. 6.

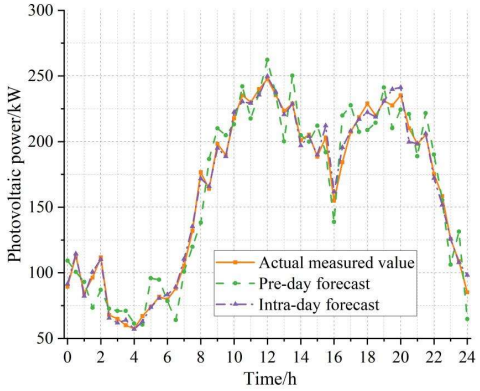

Figure 6: The pre-day, intra-day predicted and actual measured value of important load

The actual measured values of non-adjustable significant loads can be visualized in Fig. 6, and the accuracy of the predicted values regarding significant loads is also high, with 86.18% accuracy for the day-ahead predicted values and 96.34% accuracy for the intraday predicted values.

III. B. 2) Steady-state operation state simulation analysis

After completing the simulation analysis of the day-ahead and intraday scheduling strategies, in order to further verify the reliability of the microgrid system in long-term stable operation, this section conducts the simulation of the network voltage, current, and the output characteristics of the distributed power sources (DGs) under the steady state condition, which reveals the comprehensive performance of the system in the grid-connected mode.

The simulation analysis is carried out on the built simulation model of the microgrid system, and the simulation time is set to 5 s, and the step size is set to 10 us.Since the microgrid is in the grid-connected state, the frequency and voltage of the system are supported by the large power grid. Therefore, it is set in this paper that the battery as the main energy storage unit does not participate in power regulation in the grid-connected state of the microgrid. The simulation of the microgrid in stable operation state includes: the voltage and current at the network side; the grid-connected state of the combined PV battery system, PV power generation system, fuel cell, and wind power generation system, as well as the power output.

When the microgrid adopts the grid-connected operation mode, the DG connected to the microgrid does not need to bear the power fluctuation of the microgrid system. Therefore, the DGs within the microgrid system all use the PQ control mode to produce power according to the given power. Figures 7, 8, 9 and 10 show the power output curves of the combined PV storage and chemical pond system, PV power generation system, fuel cell and wind power generation system, respectively.

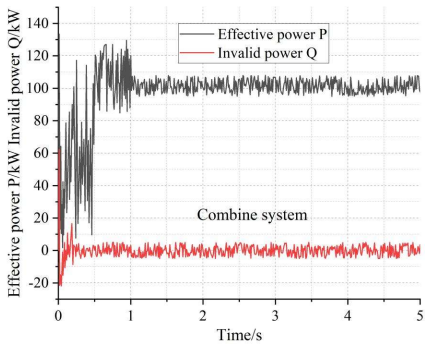

Figure 7: output power curves of combine system

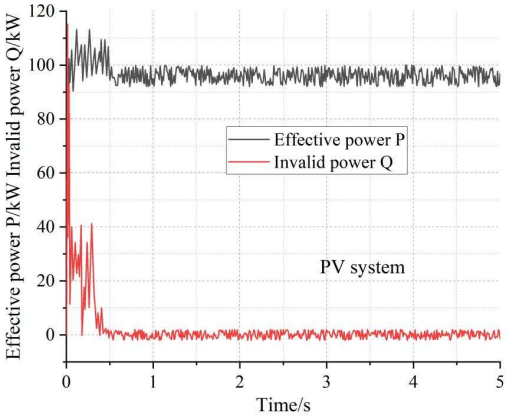

Figure 8: output power curves of PV system

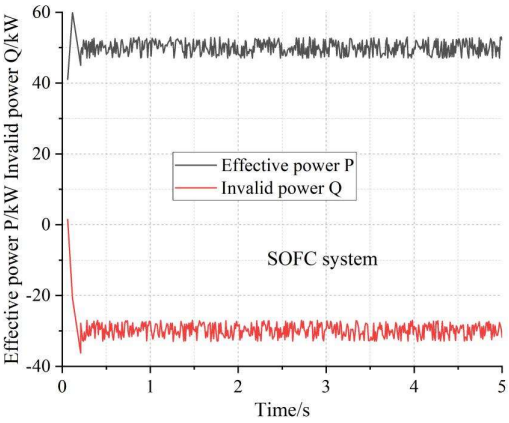

Figure 9: output power curves of SOFC system

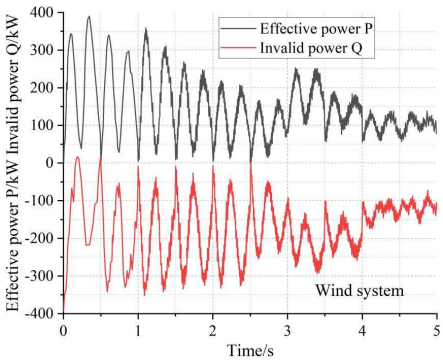

Figure 10: output power curves of PV system

From the power curves of each DG within the microgrid system at steady state in the above figure, it can be seen that each DG needs to run for a period of time to reach steady state, and the time to reach steady state varies due to the different operating characteristics of each DG. Among them, the PV battery combined system reaches steady state after 1s, and the effective power P and ineffective power Q are stabilized between 100kW and 0kW, respectively; the PV power generation system reaches steady state after 0.5s, and the effective power P and ineffective power Q are stabilized between 95kW and 0kW, respectively; the fuel cell reaches steady state after 0.3s, and the effective power P and ineffective power Q are stabilized between 50kW and - 30kW; the wind power generation system reaches steady state after 4s. Eventually, the output power of each DG is stabilized, and the simulation results at the steady state of the microgrid system verify the accuracy and validity of the microgrid system modeling.

IV. Conclusion

In this paper, the stability and flexibility challenges of new energy access in low-voltage distribution networks are systematically solved through intelligent algorithm optimization and flexible interconnection technology. The honeycomb active distribution network (HADN) realizes power mutual backup between microgrid clusters through SPIES, the fault isolation time is shortened to milliseconds, and the new energy local consumption rate is increased to more than 85%. Under the hierarchical control system, the VSC-based power interaction controller supports the cooperative operation of multiple microgrids, and the simulation shows that the system can still maintain the voltage deviation <2% and the frequency fluctuation <0.1 Hz under the complex perturbation.The accuracy of PV power prediction of the proposed method is as high as 98.86% (intra-day), and the various DGs stabilize quickly in the steady state operation (up to 4 seconds for the wind system), and the accuracy of the important load prediction is as high as 96.34%, which verifies the practicality and reliability of the model.

Funding

This work was supported by GZKJXM20240015.

References

[1] Zhao, Z., Yang, K., & Xu, Y. (2023). Low-carbon transformation of power structure under the “double carbon” goal: power planning and policy implications. Environmental Science and Pollution Research, 30(25), 66961-66977.

[2] Yi, Y., Chang, L., Wu, B., Zhao, J., Peng, H., Li, L., & Wang, A. (2024). Life Cycle Assessment of Energy Storage Technologies for New Power Systems under Dual‐Carbon Target: A Review. Energy Technology, 12(5), 2301129.

[3] Ciontea, C. I., & Iov, F. (2021). A study of load imbalance influence on power quality assessment for distribution networks. Electricity, 2(1), 77-90.

[4] Ma, K., Fang, L., & Kong, W. (2020). Review of distribution network phase unbalance: Scale, causes, consequences, solutions, and future research directions. CSEE Journal of Power and Energy systems, 6(3), 479-488.

[5] Li, Y., He, L., Liu, F., Li, C., Cao, Y., & Shahidehpour, M. (2017). Flexible voltage control strategy considering distributed energy storages for DC distribution network. IEEE Transactions on Smart Grid, 10(1), 163-172.

[6] Olivella-Rosell, P., Bullich-Massagué, E., Aragüés-Peñalba, M., Sumper, A., Ottesen, S. Ø., Vidal-Clos, J. A., & Villafáfila-Robles, R. (2018). Optimization problem for meeting distribution system operator requests in local flexibility markets with distributed energy resources. Applied energy, 210, 881-895.

[7] Razavi, S. E., Rahimi, E., Javadi, M. S., Nezhad, A. E., Lotfi, M., Shafie-khah, M., & Catalão, J. P. (2019). Impact of distributed generation on protection and voltage regulation of distribution systems: A review. Renewable and Sustainable Energy Reviews, 105, 157-167.

[8] Ibrahim, I. A., & Hossain, M. J. (2021). Low voltage distribution networks modeling and unbalanced (optimal) power flow: A comprehensive review. IEEE Access, 9, 143026-143084.

[9] Yang, J. D., & Zhao, X. T. (2024). Study on Optimization of Low-Voltage Multi-Port Flexible Interconnection Device in AC/DC Hybrid Distribution. Journal of Nanoelectronics and Optoelectronics, 19(3), 307-316.

[10] Arboleya, P., Kippke, M. A., & Kerscher, S. (2022). Flexibility management in the low-voltage distribution grid as a tool in the process of decarbonization through electrification. Energy Reports, 8, 248-256.

[11] Lynch, P., Power, J., Hickey, R., & Messervey, T. (2017). Business model strategies: Flexibility trade in emerging low voltage distribution networks. Entrepreneurship and Sustainability Issues, 4(3), 380.

[12] Oikonomou, K., Parvania, M., & Khatami, R. (2019). Deliverable energy flexibility scheduling for active distribution networks. IEEE Transactions on Smart Grid, 11(1), 655-664.

[13] Di, W., Wei, W., Shaoqu, W., Zhuofei, Y., Houtao, S., & Dan, H. (2022, October). Research and application of low-voltage flexible interconnection technology of distribution network. In 2022 Asian Conference on Frontiers of Power and Energy (ACFPE) (pp. 478-483). IEEE.

[14] Wu, T., Zheng, Y., Wu, H., Dong, H., & Wang, X. (2019). Power transfer and multi-control mode of a distribution network based on a flexible interconnected device. IEEE Access, 7, 148326-148335.

[15] Yuan, M., Li, X., Wang, F., Zhu, C. Y., & Xian, G. Q. (2024, September). Design of One New Low-Cost Flexible Interconnection of Distribution Grids and Control System. In 2024 China International Conference on Electricity Distribution (CICED) (pp. 356-360). IEEE.

[16] Li, J., Zhang, L., Zhang, B., & Tang, W. (2023). Coordinated planning for flexible interconnection and energy storage system in low-voltage distribution networks to improve the accommodation capacity of photovoltaic. Global Energy Interconnection, 6(6), 700-713.

[17] Zu, G., Wang, Y., Jiang, X., Hao, Z., & Zhang, X. (2024). Total supply capability of electricity distribution networks considering flexible interconnection of low‐voltage service transformers. IET Smart Grid, 7(4), 386-399.

[18] Yang, Y., Pei, W., Huo, Q., Sun, J., & Xu, F. (2018). Coordinated planning method of multiple micro-grids and distribution network with flexible interconnection. Applied Energy, 228, 2361-2374.